

**Electronic Supplementary Information (ESI)**

**Computational Mechanistic Insights on Ag<sub>2</sub>O as a Host for Li in Lithium-Ion Battery**

C. Hepsibah Priyadarshini<sup>1</sup>, V. Sudha<sup>1\*</sup>, S. Harinipriya<sup>2</sup>

<sup>1</sup>*Department of Chemistry, SRM Institute of Science and Technology, Kattankulathur, India, 603203*

<sup>2</sup>*Inventus BioEnergy Pvt. Ltd, Vembakkam, Chengalpattu, Tamil Nadu, India, 603111.*

*\*Corresponding Author, Department of Chemistry, SRM Institute of Science and Technology, Kattankulathur, India, 603203. Email: [sudhav1@srmist.edu.in](mailto:sudhav1@srmist.edu.in)*

**Electronic Supplementary Information (ESI) available:**

Optimization of Ag<sub>4</sub>O<sub>2</sub> supercell; Adsorption of two Li/unit cell of Ag<sub>2</sub>O at the interstitial sites; Different zones of Ag<sub>4</sub>O<sub>2</sub> supercell considered for Bader charge analysis; Validation of the choice of parameters for equilibration and thermalisation; Table depicting the mechanism of Li adsorption in various LiB hosts.

### ESI-1. Optimization of Ag<sub>4</sub>O<sub>2</sub> supercell

For the adsorption studies of Li atoms, the 2x2x3 supercell of Ag<sub>4</sub>O<sub>2</sub> consisting of four Ag<sub>2</sub>O unit cells per zone is considered. In that, the bottom two zones are fixed and atoms are relaxed in the topmost zone. The details of the optimized 2x2x3 Ag<sub>4</sub>O<sub>2</sub> surface are given as follows

Table S1 Cell parameters and bond lengths of optimised 2x2x3 surface of Ag<sub>4</sub>O<sub>2</sub>. All values are reported in Å.

a	b	c	Ag – O	Ag – Ag
9.6205400	9.6205400	24.430810	2.17 (surface)	4.09 (surface)
			2.08 (bottom zone)	3.41 (bottom zone)

### ESI-2. Adsorption of two Li/unit cell of Ag<sub>2</sub>O at the interstitial sites

Here two Li atoms are placed at the nearby interstitial sites of 2x2x3 surface of Ag<sub>4</sub>O<sub>2</sub> and optimized. Initially, it proceeds with the formation and stabilization of two Li–O contacts. As the stabilisation of Li–O bond escalates, the subsurface Ag–O bonds are ruptured whereas the surface Ag–O contacts are maintained. Hence, the separation of Ag<sub>2</sub>O unit from Ag<sub>4</sub>O<sub>2</sub> along with two Li–O contacts can be evidenced. Even though, the binding energy is found to be the lowest, Ag<sub>4</sub>O<sub>2</sub> framework is completely lost with one unit detaching itself from the rest with the arrival of two Li atoms.

Table S2 Calculated binding energy (in eV) of two Li atom(s) optimized at the interstitial sites using equation (1) and their corresponding bond lengths (in Å).

Ag–O	Ag–Ag	Li–O	Li–Ag	Binding Energy/Li (eV)
2.29	3.70 (Ag <sub>3</sub> –Ag <sub>4</sub> )	1.79	3.01	-3.56
–	2.83 (Ag <sub>1</sub> –Ag <sub>2</sub> )	(Both Li <sub>1</sub> & Li <sub>2</sub> )	(Both Ag <sub>3</sub> & Ag <sub>4</sub> )	

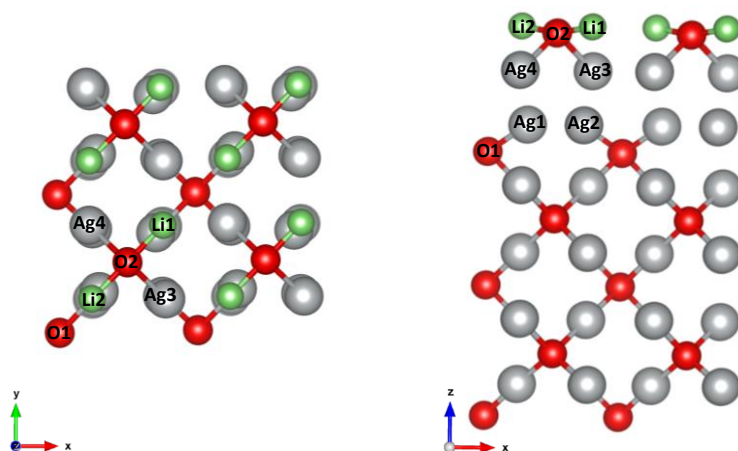


Fig. S1 The top and side views of optimised structures of two Li adsorbed on TIS. The grey, red and green circles indicate Ag, O and Li atoms respectively.

### ESI-3. Different zones of $\text{Ag}_4\text{O}_2$ supercell considered for Bader charge analysis

The various zones of  $\text{Ag}_4\text{O}_2$  as discussed in the Bader charge analysis is displayed in Fig S3. Here, Zone-I consisting of Li interacting with the  $\text{Ag}_4\text{O}_2$  unit is the region of significance since they exhibit different charge characteristics from the bulk with the arrival of Li atom. Whereas, the other two Zones shows the properties of bulk  $\text{Ag}_2\text{O}$  unit cell.

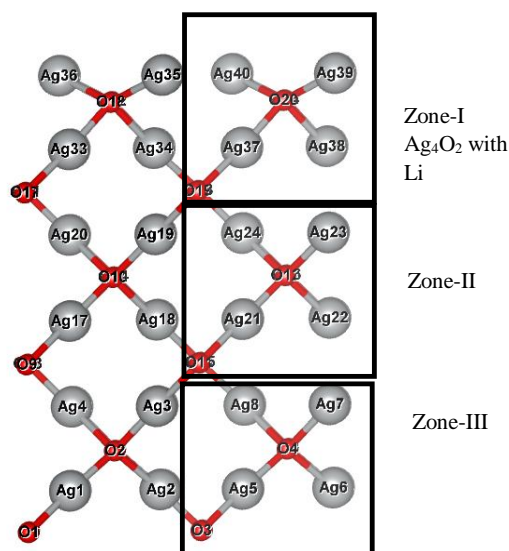


Fig. S2 The various zones in  $\text{Ag}_4\text{O}_2$  supercell

### ESI-4. Validation of the choice of parameters for equilibration and thermalisation

After the NVT simulation, the constant of motion, total, shifted electron kinetic and potential energies are plotted against the number of steps to confirm the correctness of the chosen parameters with respect to the Verlet algorithm integration. Also, the maintenance of 298K is examined by plotting Temperature (K) vs Time (ps).

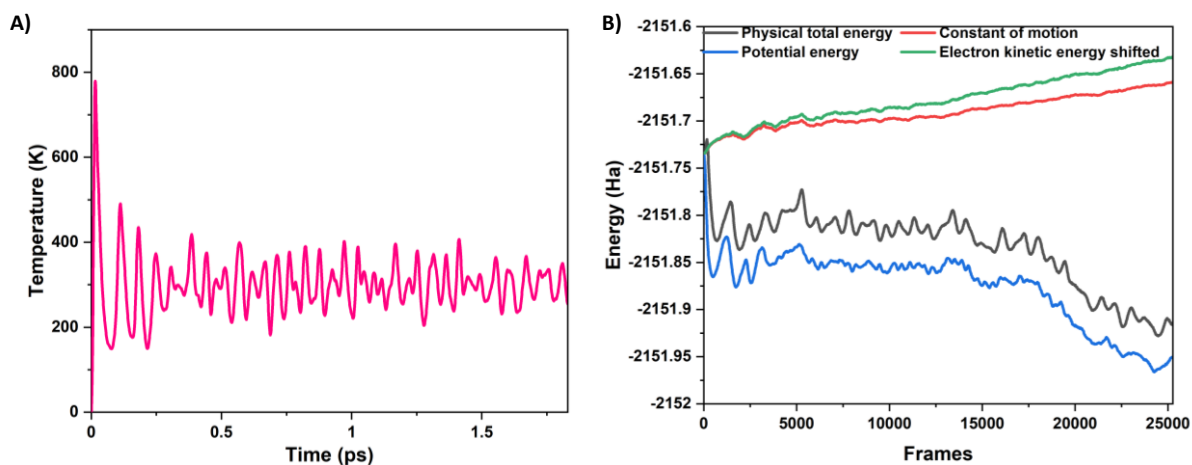


Fig. S3 The variation in (A) Energies with respect to number of steps at 298K and (B) Temperature vs Time plot depicting the thermalisation of the system

**SI-5. Table depicting the mechanism of Li adsorption in various LiB hosts**

Table S3 Comparison of the mechanisms followed by different metal oxides and fluorides in LiBs based on their methodology

MATERIAL	MECHANISM	METHOD
SnO <sub>2</sub> <sup>1</sup>	Conversion and Alloying	Experimental
SnO <sub>2</sub> <sup>2</sup>	Alloying and Conversion	DFT
Fe <sub>2</sub> O <sub>3</sub> and Fe <sub>3</sub> O <sub>4</sub> <sup>3</sup>	Conversion	Experimental
Cu <sub>2</sub> O <sup>4</sup>	Alloying and Conversion	DFT
FeF <sub>2</sub> , FeF <sub>3</sub> <sup>5</sup>	Intercalation and Conversion	DFT
ZnO <sup>6</sup>	Conversion and alloying	Experimental
ZnO <sup>7</sup>	Dissociative mechanism	DFT
AgO <sup>8</sup>	Conversion	Experimental
CuO <sup>9</sup>	Conversion	Experimental
NiO <sup>10</sup>	Conversion	Experimental and DFT

## References

- (1) Ferraresi, G.; Villevieille, C.; Czekaj, I.; Horisberger, M.; Novák, P.; El Kazzi, M. SnO<sub>2</sub> Model Electrode Cycled in Li-Ion Battery Reveals the Formation of Li<sub>2</sub>SnO<sub>3</sub> and Li<sub>8</sub>SnO<sub>6</sub> Phases through Conversion Reactions. *ACS Appl. Mater. Interfaces* **2018**, *10*, 8712–8720.
- (2) Cheng, Y.; Nie, A.; Gan, L. Y.; Zhang, Q.; Schwingenschlögl, U. A Global View of the Phase Transitions of SnO<sub>2</sub> in Rechargeable Batteries Based on Results of High Throughput Calculations. *J. Mater. Chem. A* **2015**, *3*, 19483–19489.
- (3) Jing-San, Xu.; Ying-Jie, Zhu.; Monodisperse Fe<sub>3</sub>O<sub>4</sub> and  $\Gamma$ -Fe<sub>2</sub>O<sub>3</sub> Magnetic Mesoporous Microspheres as Anode Materials for Lithium-Ion Batteries. *Appl. Mater. interfaces* **2012**, *4*, 4752–4757.
- (4) Kiran, G. K.; Periyasamy, G.; Kamath, P. V. Role of Alloying in Cu<sub>2</sub>O Conversion Anode for Li-Ion Batteries . *Theor. Chem. Acc.*, **2019**, 138,23-1-10.
- (5) Ma, Y.; Garofalini, S. H. Atomistic Insights into the Conversion Reaction in Iron Fluoride: A Dynamically Adaptive Force Field Approach. *J. Am. Chem. Soc.* **2012**, *134*, 8205–8211.
- (6) Yudha, C. S.; Hutama, A. P.; Rahmawati, M.; Widiyandari, H.; Nursukatmo, H.; Nilasary, H.; Oktaviano, H. S.; Purwanto, A. Synthesis and Characterization of ZnO from Thermal Decomposition of Precipitated Zinc Oxalate Dihydrate as an Anode Material Li-Ion Batteries. *Energies.*, **2021**, *14*,5980-1-13.
- (7) Carvalho, A.; Alkauskas, A.; Pasquarello, A.; Tagantsev, A. K.; Setter, N. A Hybrid Density Functional Study of Lithium in ZnO: Stability, Ionization Levels, and Diffusion. *Phys.Rev.B.*, **2009**, *80*, 1–12.
- (8) Li, H.; Wang, Y.; He, P.; Zhou, H. A Novel Rechargeable Li-AgO Battery with Hybrid Electrolytes. *Chem.Commun.* **2010**, *46*, 2055–2057.
- (9) Park, S. H.; Lee, W. J. Hierarchically Mesoporous CuO/Carbon Nanofiber Coaxial Shell-Core Nanowires for Lithium Ion Batteries. *Sci.Rep.* **2015**, *5*, 1–13.
- (10) He, K.; Lin, F.; Zhu, Y.; Yu, X.; Li, J.; Lin, R.; Nordlund, D.; Weng, T. C.; Richards, R. M.; Yang, X. Q.; Doeff, M. M.; Stach, E. A.; Mo, Y.; Xin, H. L.; Su, D. Sodiation Kinetics of Metal Oxide Conversion Electrodes: A Comparative Study with Lithiation. *Nano Lett.* **2015**, *15*, 5755–5763.